Ⓔ

Strong-Motion Observations of the 2017 M_s 7.0 Jiuzhaigou Earthquake: Comparison with the 2013 M_s 7.0 Lushan Earthquake

by Yefei Ren, Hongwei Wang, Peibin Xu, Yadab P. Dhakal, Ruizhi Wen, Qiang Ma, and Peng Jiang

ABSTRACT

Strong-motion recordings observed during the M_s 7.0 Jiuzhaigou earthquake, which occurred on 8 August 2017 in western China, were used to reveal the underlying source, propagation path, and site effects in comparison with observations from the 2013 Lushan earthquake of identical magnitude (M_s 7.0). The similar V_{S30} distributions at the strong-motion stations considered in both events reflect approximately consistent site effects. Amplitudes of short- and intermediate-period ground motions (e.g., peak ground accelerations, peak ground velocities, and pseudospectral accelerations [PSAs] at $T = 0.2$ and 2.0 s) observed in the Jiuzhaigou event were smaller than in the Lushan earthquake at sites with a Joyner–Boore distance (R_{JB}) of < 200 km, but their amplitudes were similar at far-field sites ($R_{JB} > 200$ km). However, irrespective of R_{JB}, larger amplitudes of long-period ground motions (e.g., PSAs at $T = 5.0$ s) were observed in the Jiuzhaigou earthquake compared with the Lushan event. This study revealed that different fault styles (strike slip for the Jiuzhaigou event and reverse slip for the Lushan event), and different centroid depths could be two reasons for the period-dependent differences of ground motions between the two earthquakes. Analysis of within-event residuals suggested that the Jiuzhaigou region exhibited slower anelastic attenuation for short- and intermediate-period ground motions than the Lushan region, but the anelastic attenuations for long-period ground motions of both regions were similar. The durations of ground motions generated by both earthquakes were found comparable, as were the dependences on distance in both seismogenic regions.

Electronic Supplement: Table containing information of the strong-motion stations in the Jiuzhaigou earthquake considered in this study.

INTRODUCTION

The M_s 7.0 Jiuzhaigou earthquake, which struck western China at 21:19:46 (Beijing time) on 8 August 2017, was the most recent in a series of destructive events in the region, for example, the M_s 8.0 Wenchuan earthquake in 2008, the M_s 7.0 Lushan earthquake in 2013, and the M_s 6.5 Ludian earthquake in 2014. The Jiuzhaigou event caused 25 fatalities and 525 injuries (derived from the official report of China Earthquake Administration [CEA]; see Data and Resources), which resulted primarily from seismically induced geological hazards, such as landslides and rockfalls in the Jiuzhaigou region and its neighboring municipalities, rather than from failures of engineering structures. After five days of intensive field investigation, the CEA officially released the seismic intensity map (see Data and Resources); the maximum intensity reached IX on the Chinese seismic intensity scale (GB/T 17742, 2008; equivalent to modified Mercalli intensity [MMI] IX), the same level as the 2013 Lushan earthquake. The China Earthquake Networks Center reported that this earthquake had a shallow focal depth of 20 km, an epicenter at 33.20° N, 103.82° E, and surface magnitude of M_s 7.0. The Global Centroid Moment Tensor (CMT) Project provided the value of the moment magnitude as $M_w = 6.5$.

The Jiuzhaigou earthquake occurred on the northern segment of the Huya fault, which is a north-northwest–south-southeast-trending left-lateral strike-slip fault that belongs to one of the tail structures at the easternmost end of the eastern Kunlun fault zone (Xu *et al.*, 2017). According to an inversion of the rupture process (Zhang *et al.*, 2017), this event ruptured an approximately vertical plane with dimensions of 40×20 km toward the west-southwest (highlighted by the green-filled rectangle in Fig. 1), which caused an average stress drop of 3.8 MPa on the ruptured zone (Wang *et al.*, 2017). The Huya fault has been very active seismically in recent decades, particularly in the 1970s when the 1973 M 6.2 Huanglong earthquake and 1976 Songpan earthquake swarm ($M = 7.2$, 6.7, and 7.2) occurred (highlighted in Fig. 1). The 2017 Jiuzhaigou event was followed immediately by numerous aftershocks: 36 with magnitudes of $M \geq 3.0$ and 4 with magnitudes of

 doi: 10.1785/0220170238

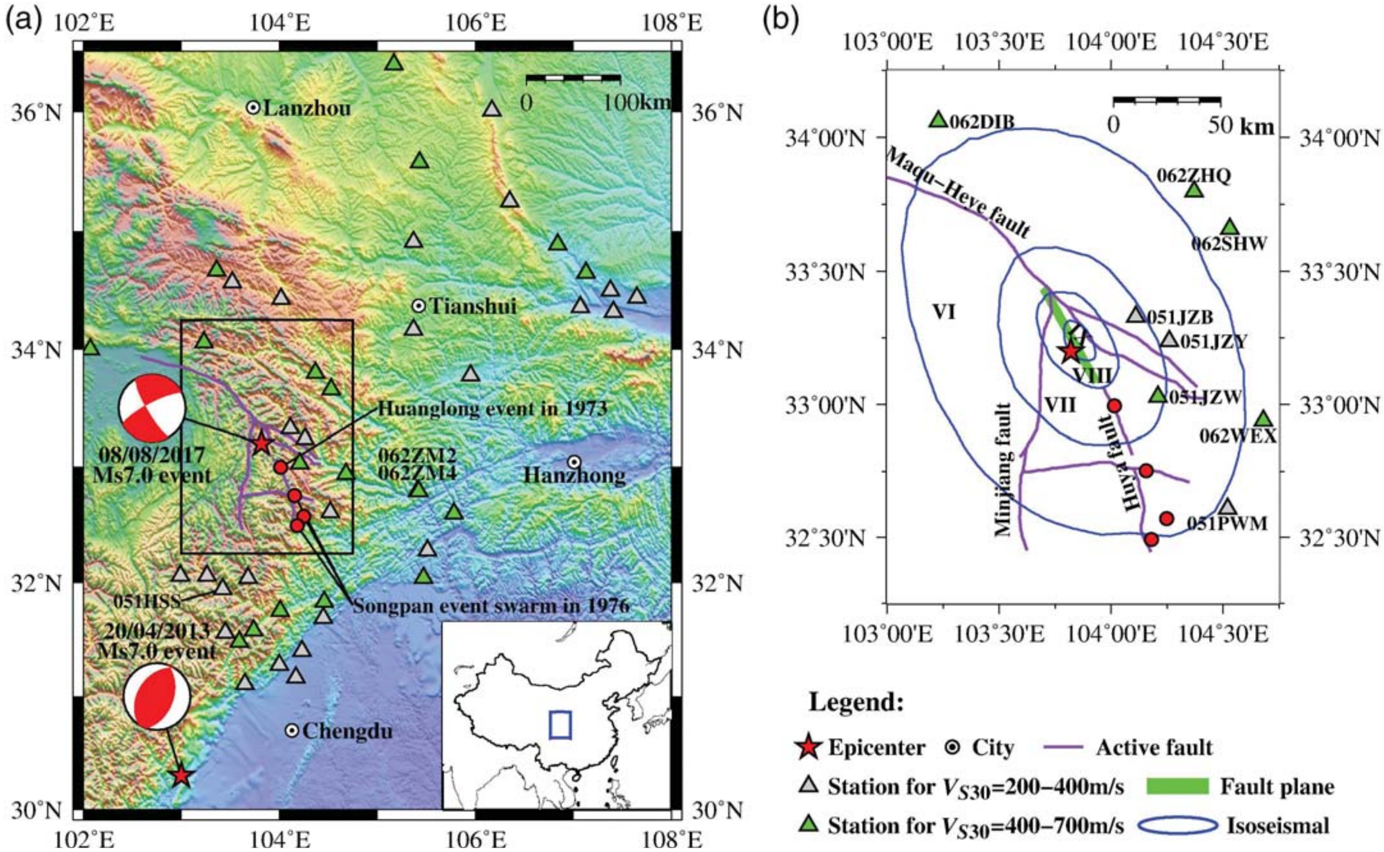

▲ **Figure 1.** (a) Locations of strong-motion stations triggered in the Jiuzhaigou earthquake for R_{JB} < 400 km. These stations are separated into two groups (represented by gray and green triangles) according to the range of V_{S30}. Stations 062ZM2 and 062ZM4 almost at the same location constitute a local terrain array. Purple lines indicate active faults in the proximity of the epicenter (represented by the red star). The focal mechanism plots for both the Jiuzhaigou and the Lushan earthquakes were drawn according to the focal mechanisms provided by the Global Centroid Moment Tensor Project. Four large historical earthquakes that occurred on the Huya fault are represented by red-filled circles, that is, the 1973 M 6.2 Huanglong earthquake and 1976 Songpan earthquake swarm ($M = 7.2$, 6.7, and 7.2). (b) Eight stations with R_{JB} < 100 km, enclosed within the rectangle with their station codes. Blue contours represent isoseismals. The green-filled area indicates the surface projection of the fault plane derived from Zhang *et al.* (2017).

$M \geq 4.0$ but none with magnitude of $M \geq 5.0$ (by the end of 8 October 2017).

Some dozens of strong-motion recordings were collected during the Jiuzhaigou earthquake by China's National Strong Motion Observation Networks System (NSMONS). Although the total number of recordings acquired was modest, and the maximum peak ground acceleration (PGA) recorded was only 177.68 cm/s^2, the strong-motion observations of this earthquake could compensate for the lack of recordings from other large destructive events in China's strong-motion database. Thus, these data could contribute considerably to future systematic studies of earthquake engineering and seismology, for example, through the development of ground-motion prediction equations (GMPEs) for western China. There are only two events of magnitude similar to or larger than that of the Jiuzhaigou earthquake for which NSMONS collected considerable numbers of strong-motion recordings, that is, the 2008 M_s 8.0 Wenchuan earthquake and the 2013 M_s 7.0 Lushan earthquake (Li *et al.*, 2008; Wen and Ren, 2014).

The Jiuzhaigou earthquake was located ~300 km north-northeast of the 2013 Lushan earthquake (Fig. 1). Both events were scaled as having the same surface magnitude (i.e., M_s 7.0) and similar moment magnitudes (M_w 6.6 for the Lushan event and M_w 6.5 for the Jiuzhaigou event, as derived from the Global CMT Project) but different rupture mechanisms (strike slip for the Jiuzhaigou event with strike/dip/rake $= 150°/78°/-13°$ and reverse dip slip for the Lushan event with strike/dip/rake $= 212°/40°/100°$). Here, we present an overview of the strong-motion observations from the Jiuzhaigou earthquake, and we analyze the characteristics of some ground-motion intensity measures (IMs), that is, PGA, peak ground velocity (PGV), 5% damped pseudospectral acceleration (PSA), and significant duration (D_{SR}). These IMs are compared both with those observed in the Lushan earthquake and with predicted values estimated by GMPEs.

OBSERVED STRONG-MOTION RECORDINGS

Overview of Recordings

Overall, 66 NSMONS stations were triggered during the Jiuzhaigou earthquake within the Joyner–Boore distance (R_{JB}) of up to 600 km. The values of R_{JB} and rupture distance (R_{rup}) were calculated based on the ruptured fault plane inverted by Zhang *et al.* (2017), as shown in Figure 1. The locations of 44 stations with $R_{JB} < 400$ km are plotted in Figure 1. Recordings obtained from 42 of these stations were used to analyze the IM characteristics in this study. The two excluded stations (062ZM2 and 062ZM4) constitute a local terrain array. All 42 recordings were processed using a Butterworth filter with a bandwidth of 0.1–30.0 Hz to achieve reliable estimations of the PGAs, PGVs, and spectral ordinates of interest to engineers (Ⓔ Table S1, available in the electronic supplement to this article). To provide useful information for comparison with the estimations of the GMPEs, the values of R_{JB} and R_{rup} are also listed in Ⓔ Table S1.

The processed acceleration and velocity time series obtained at three near-fault stations for $R_{JB} \sim 30$ km (i.e., 051JZB, 051JZW, and 051JZY) are presented in Figure 2. The maximum PGA (177.68 cm/s^2) and PGV (6.66 cm/s) were recorded in the north–south component of 051JZB, the station closest to the epicenter. Only the 051JZB station recorded PGAs that exceeded 100 cm/s^2 in the Jiuzhaigou earthquake. Compared with the Lushan earthquake (68 accelerometer components recorded PGAs of > 100 cm/s^2; maximum value = 1005.3 cm/s^2 (Wen and Ren, 2014)), the Jiuzhaigou event generated relatively small ground motions. This could be one of the reasons for the absence of substantial damage caused to engineering structures, as revealed in postearthquake investigations (Han *et al.*, 2018).

During the 2013 Lushan earthquake, 121 strong-motion recordings were obtained by NSMONS stations. Of these, 91 with $R_{JB} < 400$ km were adopted in this study for comparison with those observed in the Jiuzhaigou earthquake. The values of the IMs of the Lushan earthquake were provided by Wen and Ren (2014), together with the distance metrics R_{JB} and R_{rup}. Figure 3 shows the R_{JB} distributions of strong-motion recordings observed in both earthquakes considered in this study. Most recordings in both events were acquired at stations with $R_{JB} > 100$ km. Nine recordings from stations with $R_{JB} <$ 20 km were collected in the Lushan earthquake, but none was obtained from the Jiuzhaigou earthquake. There were 8 and 17 recordings in the Jiuzhaigou and Lushan earthquakes, respectively, within the R_{JB} range of 20–100 km, accounting for similar proportions (~20%) of all the recordings of both events considered here. The station codes of the eight stations with $R_{JB} < 100$ km in the Jiuzhaigou earthquake are marked in Figure 1.

Site Conditions of Strong-Motion Stations

As vital preparation for the comparison between the observed and predicted IMs, the site conditions of all strong-motion stations analyzed in the Jiuzhaigou and Lushan earthquakes were evaluated. Two Next Generation Attenuation-West 2 (NGA-West2) models for predicting ground motions of the shallow crustal earthquakes, the Abrahamson *et al.* (2014; hereafter, ASK14) and Boore *et al.* (2014; hereafter, BSSA14) models, were used to provide predictions in this study. In both models, the time-weighted average shear-wave velocity over the upper 30 m (V_{S30}) was regarded as representative in reflecting the impact of site effects on ground motion. The V_{S30} values in our study were not all measured from the velocity profile with depth $z_p \geq 30$ m. The V_{S30} values for stations included in the NGA-West2 site database were derived from the recommended values in this database (Seyhan *et al.*, 2014). In this database, for stations with available borehole data to profile depth z_p, the recommended V_{S30} values were inferred from the V_{Sz} values (the time-weighted average shear-wave velocity to profile depth z_p) according to the V_{S30}–V_{Sz} linear model of Yu and Silava (in the Pacific Earthquake Engineering Research Center report of Ancheta *et al.*, 2013). Otherwise, the inferred V_{S30} from proxies that incorporate geomorphological- or terrain-based metrics, including geotechnical category, ground slope, terrain-based categories, was used as the recommended value. For the stations not included in this database, we inferred V_{S30} values based on an empirical relationship between the site classification defined in the Code for Seismic Design of Buildings in China (GB 50011, 2010) and V_{S30}.

Lyu and Zhao (2007) proposed that V_{S30} is > 510 m/s for class I sites, 260–510 m/s for class II sites, 150–260 m/s for class III sites, and < 150 m/s for class IV sites. We collected V_{S30} values for 211 strong-motion stations in western China (most are in Sichuan Province, others in Yunnan, Gansu, Shanxi, Ningxia, and Qinghai Provinces) from the NGA-West2 site database. These stations were classified into three classes: 34 as class I, 152 as class II, and 25 as class III, according to the above-mentioned V_{S30} ranges, as shown in Figure 4. The mean V_{S30} value for the stations in each site class was calculated, which produced values of 575.33 m/s for class I, 369.81 m/s for class II, and 236.33 m/s for class III. These values approximately represent the mean V_{S30} values for the three site classes in western China.

For NSMONS stations, Ji *et al.* (2017) designed a flowchart to classify their site classes based on comprehensive consideration of peak period, amplitude, and shape of the horizontal-to-vertical spectral ratio (HVSR) curves. In our study, their proposed method was used to determine the site classes for stations not included in the NGA-West2 site database. The HVSR was calculated using the observed recordings at these stations. Then the V_{S30} value of each station was assigned by the mean of the corresponding site class. The V_{S30} values for all 42 stations considered in the Jiuzhaigou earthquake are listed in Ⓔ Table S1. The V_{S30} values for a total of 23 stations were directly derived from the NGA-West2 database. The remaining 19 ones were inferred from the empirical relationship described in our study. Figure 5 shows histograms of the V_{S30} values for the sites of the strong-motion stations considered in the Jiuzhaigou and Lushan earthquakes. The two events show

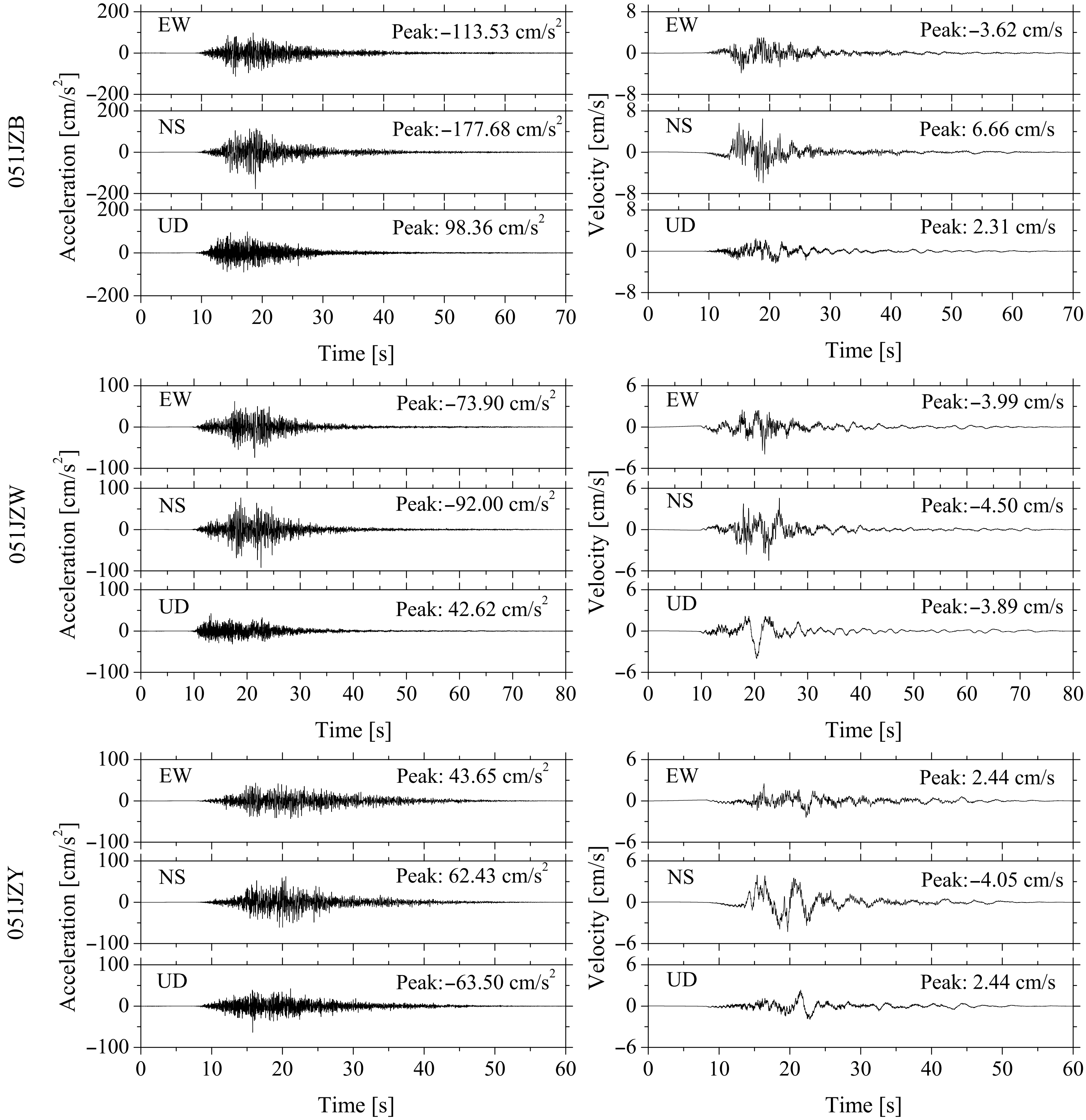

▲ **Figure 2.** Processed acceleration and velocity time series for the east–west (EW), north–south (NS), and up–down (UD) components recorded by three near-fault stations: 051JZB, 051JZW, and 051JZY. The peak ground acceleration (PGA) and peak ground velocity (PGV) are marked in the top-right corner of each panel.

similar distributions with values of V_{S30} predominantly within the 350–400 m/s range. In fact, some stations recorded both events, while those stations that recorded a single event are located mostly within the same region. Most stations could be classified as class II sites according to the 260–510 m/s V_{S30} range recommended by Lyu and Zhao (2007).

PGA, PGV, and PSA

The observed PGAs and PGVs from the Jiuzhaigou earthquake were compared with the medians predicted by the ASK14 and BSSA14 models, respectively, as shown in Figure 6 and PSAs at periods of 0.2, 2.0, and 5.0 s as shown in Figure 7. The strike-slip fault type and $M_w = 6.5$ were fixed in both models and

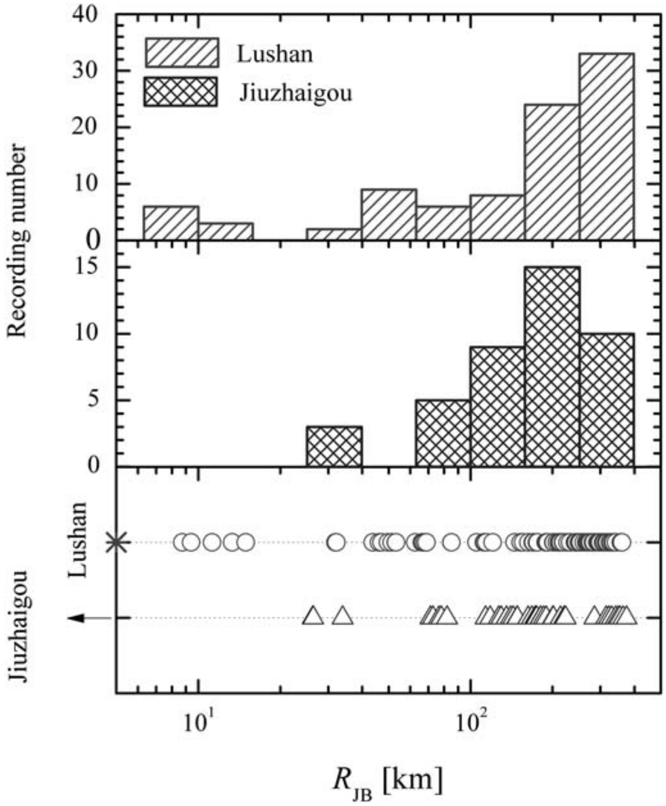

▲ **Figure 3.** Joyner–Boore distance (R_{JB}) distributions of the 42 and 91 recordings obtained in the Jiuzhaigou and Lushan earthquakes, respectively, considered in this study. The cross on the vertical axis ($R_{JB} = 5$ km) represents the four recordings obtained at stations with $R_{JB} = 0$ km in the Lushan earthquake.

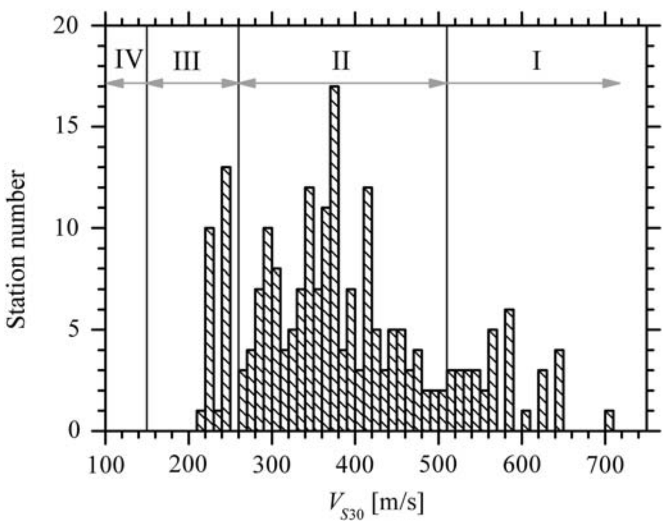

▲ **Figure 4.** Histogram of V_{S30} values for 211 strong-motion stations in western China derived from the Next Generation Attenuation-West 2 (NGA-West2) site database. Vertical lines represent the boundaries of the V_{S30} ranges proposed by Lyu and Zhao (2007) for different site classes, as defined in the Chinese seismic code, that is, < 150 m/s for class IV, 150–260 m/s for class III, 260–510 m/s for class II, and > 510 m/s for class I.

the regional adjustment of anelastic attenuation for China was considered. The V_{S30} value of each station site was considered to represent the site-effect term. The effect of $Z_{TOR} = 0$ km (the vertical depth to the shallowest point on the rupture surface) was considered in the ASK14 model. However, the sediment thickness effects were not included in predictions for both models because most stations are located on the mountains area (see Fig. 1). Considering the compatibility between these observed and predicted IMs, the RotD50 parameters were calculated for each recording and the results for PGA, PGV, and PSAs at periods of 0.2, 0.5, 1.0, 2.0, and 5.0 s are listed in Ⓔ Table S1. The RotD50 indicates the 50th percentile of the median amplitude of the horizontal ground motions over all nonredundant rotations, as proposed by Boore (2010).

Figures 6 and 7 show that the predicted medians of PGA and PSA at period of 0.2 s do not show obvious discrepancies between the models. However, much higher predictions of PGV and PSAs at periods of 2.0 and 5.0 s at regional distances for $R_{JB} > 200$ km were provided by the BSSA14 model than the ASK14 model. Except for the good predication of PSA at period of 5.0 s provided by the ASK14 model, the PGA, PGV, and PSAs at periods of 0.2 and 2.0 s in the Jiuzhaigou earthquake were noticeably overestimated by both prediction models. The BSSA14 model provided much more significant

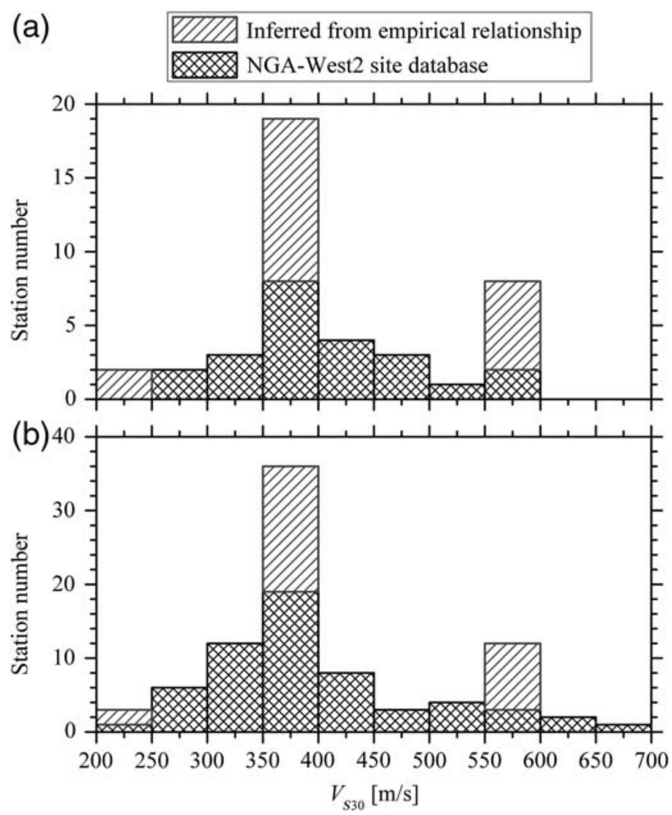

▲ **Figure 5.** Histograms of V_{S30} values for strong-motion stations considered in this study: (a) the Jiuzhaigou earthquake and (b) the Lushan earthquake. The V_{S30} values derived directly from the NGA-West2 site database and inferred from the empirical relationship between site class and V_{S30} are represented by different fill patterns.

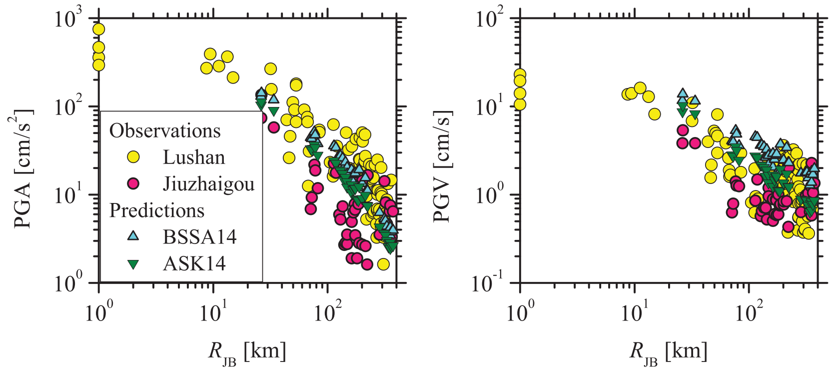

▲ **Figure 6.** Comparisons of the observed PGAs and PGVs in the Jiuzhaigou earthquake with predictions estimated by both the Abrahamson *et al.* (2014; hereafter, ASK14) and Boore *et al.* (2014; hereafter, BSSA14) models, together with observations from the Lushan earthquake. PGAs and PGVs observed at four stations with $R_{JB} = 0$ km in the Lushan earthquake are plotted on the vertical axis (i.e., $R_{JB} = 1$ km).

overestimations for PGV and PSAs at periods of 2.0 and 5.0 s with $R_{JB} > 200$ km.

We also compared the observed PGAs and PGVs in the Jiuzhaigou earthquake with those observed in the Lushan earthquake (Fig. 6). It shows that both the PGAs and the PGVs observed in the Jiuzhaigou earthquake for $R_{JB} < 200$ km were generally smaller than in the Lushan earthquake. However, the PGAs and PGVs at far-field sites, that is, $R_{JB} > 200$ km, were approximately consistent in both earthquakes. The same tendency could be observed for PSAs at short and intermediate periods (e.g., 0.2 and 2.0 s), as shown in Figure 7. However, interestingly, the opposite tendency was observed for long-period PSAs (e.g., 5.0 s), that is, the observations in the Jiuzhaigou earthquake were generally larger than in the Lushan earthquake.

The total residuals, expressed as the observed values minus the median values predicted by both the ASK14 and BSSA14 models on the natural logarithmic scale, were calculated for the PGAs and PSAs at periods up to 5 s. Different with the Jiuzhaigou earthquake, the predicted medians for the Lushan earthquake were calculated using the following options: (1) $M_w = 6.6$; (2) reverse-slip fault type; (3) regional adjustment of anelastic attenuation for China; (4) $Z_{TOR} = 0$ km in the ASK14 model; and (5) dip, location over the rupture, depth, and distance off the ends of the rupture (referring to the fault model of Wang *et al.*, 2013) for representing the hanging-wall effects in the ASK14 model.

The total residuals were then separated into between-event residuals (δB) and within-event residuals (δW), as described by Al Atik *et al.* (2010). The δB term represents the average deviation of observed ground motion associated with an earthquake to the median predicted by the GMPE, which reflects event-to-event variability. The δW term represents the degree of misfit between an individual observation at a station and the earthquake-specific median prediction. The regional adjustments of anelastic attenuation for China in both models were all established based on the strong-motion recordings from the 2008 Wenchuan earthquake sequence. The Wenchuan earthquake sequence occurred on the central and northern Longmen Shan fault belt, the boundary between the eastern Tibet plateau and Sichuan basin. The Lushan event occurred on the southern Longmen Shan fault belt, while the Jiuzhaigou event occurred on the tail structures at the easternmost end of the eastern Kunlun fault zone within the eastern Tibet plateau. Although the locations for both events and the Wenchuan earthquake sequence are relatively close, substantial differences in crustal structure in these regions have been reported by some studies (e.g., Wang *et al.*, 2007; Li *et al.*, 2012). To ensure the δW values appropriately reveal the potential difference of anelastic attenuation effects between both events, the δB values were calculated using recordings only with $R_{JB} < 80$ km. As suggested by previous studies (e.g., Abrahamson *et al.*, 2014; Boore *et al.*, 2014), at distances greater than 80 km, differences in

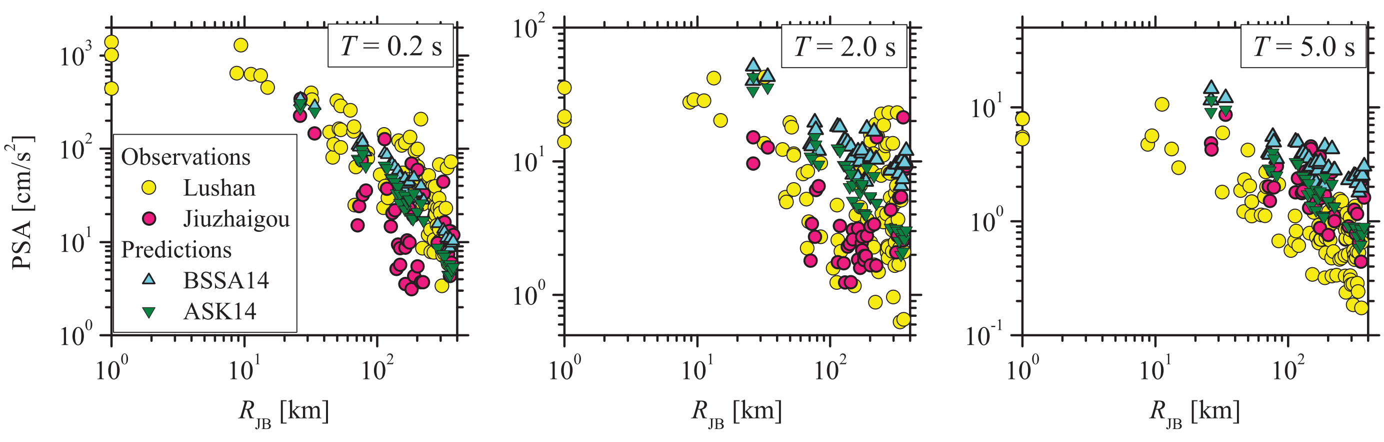

▲ **Figure 7.** Same as Figure 6 but for pseudospectral accelerations (PSAs) at periods of 0.2, 2.0, and 5.0 s, respectively.

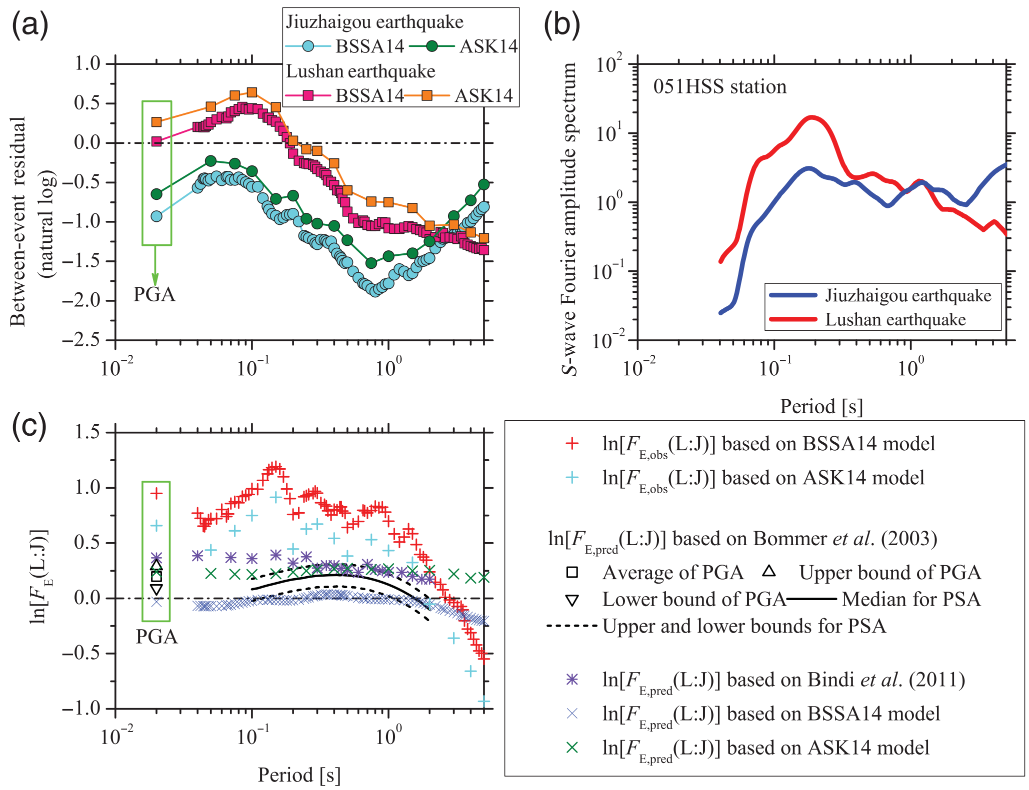

▲ **Figure 8.** (a) Between-event residuals for PGA and PSAs at periods up to 5.0 s for the Jiuzhaigou and Lushan earthquakes based on the BSSA14 and ASK14 ground-motion prediction equation (GMPE) models, respectively. (b) *S*-wave Fourier amplitude spectra recorded at station 051HSS in the Jiuzhaigou and Lushan earthquakes. The similar R_{JB} distances for this station allow investigation of the different source effects between both events. (c) Comparison of the source term of the ground motions from the Jiuzhaigou and Lushan earthquakes, represented by its ratio of the Jiuzhaigou earthquake to the Lushan event. The empirical values were provided by other studies, for example, Bommer *et al.* (2003), Bindi *et al.* (2011), Boore *et al.* (2014), and Abrahamson *et al.* (2014).

crustal structure can have significant effects on the ground motions leading to a change in the attenuation at large distances (e.g., the anelastic attenuation).

Figure 8a shows the computed values of δB for the Jiuzhaigou and Lushan earthquakes, reflecting the differences between the source effects of both earthquakes on the ground motions. Generally, the δB values from the ASK14 model were slightly larger than from the BSSA14 model for both events, indicating relatively lower predictions of source term provided by the ASK14 model. The δB values were all negative for PGA and PSAs within the analyzed periods between 0.04 and 5 s for the Jiuzhaigou earthquake, indicating overprediction of the source term in both models for this event. For the Lushan earthquake, positive δB values for PGA and PSAs at $T \le 0.2$ s, and negative δB values for PSAs at $T > 0.2$ s indicate underprediction of the source effects on short-period ground motions but overprediction on intermediate- and long-period ground motions.

The δB values for PGA and PSAs at $T < 2.5$ s for the Lushan earthquake were considerably larger than for the Jiuzhaigou earthquake, but smaller for PSAs at periods of 2.5–5.0 s. We compared the *S*-wave Fourier amplitude spectra recorded at station 051HSS in the Jiuzhaigou and Lushan earthquakes, as shown in Figure 8b. The differences between the spectra of both events are evident. The R_{JB} distances are approximate for this station in both events, that is, 135.48 km for the Jiuzhaigou earthquake and 152.65 km for the Lushan earthquake. Therefore, excluding site and path effects, source effects might have been one primary cause of such differences. The tendency of the spectra difference shown in Figure 8b is approximately consistent with that of δB shown in Figure 8a, confirming that source effects caused the larger long-period ground motions but smaller short- and intermediate-period ground motions in the Jiuzhaigou earthquake compared with the Lushan earthquake.

To reveal the source difference between the Jiuzhaigou and Lushan events, we compared only the source term of the observed ground motions from both events. According to the definition of δB, the differences of the δB values between both earthquakes could be represented by

$$\delta B_L - \delta B_J = [\ln(F_{E,obs,L}) - \ln(F_{E,pred,L})] - [\ln(F_{E,obs,J}) - \ln(F_{E,pred,J})], \quad (1)$$

in which subscripts L and J represent the Lushan and Jiuzhaigou earthquakes, respectively. Here, $\ln(F_{E,obs,L})$ and $\ln(F_{E,obs,J})$ represent the source term of the ground motions observed in the Lushan and Jiuzhaigou earthquakes, respectively. The terms $\ln(F_{\mathrm{E,pred,L}})$ and $\ln(F_{\mathrm{E,pred,J}})$ represent the source term of the ground motions predicted using the GMPE models for the Lushan and Jiuzhaigou earthquakes, respectively. According to equation (1), the difference of the source term for the observed ground motions between both earthquakes, $\ln(F_{\mathrm{E,obs,L}}) - \ln(F_{\mathrm{E,obs,J}})$, denoted by $\ln[F_{\mathrm{E,obs}}(\mathrm{L:J})]$, could be approximately given by:

$$\ln[F_{\mathrm{E,obs}}(\mathrm{L:J})] = (\delta B_{\mathrm{L}} - \delta B_{\mathrm{J}}) + [\ln(F_{\mathrm{E,pred,L}}) - \ln(F_{\mathrm{E,pred,J}})]. \quad (2)$$

For the BSSA14 model, the source term was derived from the source function given by equation (2) of Boore *et al.* (2014). The dummy variables were used to reflect the effects of fault types in this function. For this model, $\ln(F_{\mathrm{E,pred,L}}) - \ln(F_{\mathrm{E,pred,J}})$, denoted by $\ln[F_{\mathrm{E,pred}}(\mathrm{L:J})]$, is approximately close to zero, as shown in Figure 8c. For the source term of the ASK14 model, the hanging-wall model was developed to reflect the effects of reverse-slip event on hanging-wall stations. Therefore, for some stations located at hanging wall in the Lushan earthquake, we calculated $\ln(F_{\mathrm{E,pred,L}})$ particularly considering the hanging-wall effect. The resultant $\ln[F_{\mathrm{E,pred}}(\mathrm{L:J})]$ averaged over these stations is approximately close to 0.25.

Figure 8c shows that $\ln[F_{\mathrm{E,obs}}(\mathrm{L:J})]$ is greater than zero for short- and intermediate-period PSAs ($T < 2.0$ s) but smaller than zero for long-period PSAs ($T > 2.0$ s). The decline trend with respect to period is almost the same as the resulting $\ln[F_{\mathrm{E,pred}}(\mathrm{L:J})]$ from other studies, that is, Bommer *et al.* (2003) and Bindi *et al.* (2011), although the amplitudes in our study were considerably larger. This is in accordance with the observations reported by some previous studies (e.g., Bommer *et al.*, 2003) that a reverse-slip earthquake is generally expected to produce ground motions with greater amplitudes at short and intermediate periods than a strike-slip event but with lower amplitudes at long periods. In Figure 8c, the $\ln[F_{\mathrm{E,pred}}(\mathrm{L:J})]$ values for the GMPE model of Bommer *et al.* (2003) were calculated according to equation (9) and coefficients in table V in their study. For the $\ln[F_{\mathrm{E,pred}}(\mathrm{L:J})]$ values given by the GMPE model of Bindi *et al.* (2011), the magnitude function (equation 3 in their study) and the functional form F_{sof} reflecting the style-of-faulting correction were applied to represent the source term. Through the above analysis, the period-dependent differences of the ground motions between the two earthquakes, shown in Figures 6 and 7, might be attributable to the different styles of fault rupture, that is, strike slip for the Jiuzhaigou earthquake and reverse slip for the Lushan earthquake (see Fig. 1 for the focal mechanisms of the events). Furthermore, the different centroid depth between both events is probably another attribution. According to the previous studies, two earthquakes show the very different centroid depth, ~5 km for the Jiuzhaigou event (Yi *et al.*, 2017) but > 10 km for the Lushan event (Han *et al.*, 2014). The shallower Jiuzhaigou event may generate the stronger surface wave with the longer period phase.

We calculated the δW values in both earthquakes by subtracting δB from the total residual based on the ASK14 and BSSA14 models, respectively. Figure 9a shows the δW values against R_{JB} for PGA and PSAs at periods of 0.2, 2.0, and 5.0 s in the Jiuzhaigou and Lushan earthquakes. Except for the PGA in Lushan event and PSA at period of 5.0 s in both events, the strong dependence of the δW on R_{JB} values was revealed by the significantly upward trends.

Following the study of Boore *et al.* (2014), we also fitted a linear expression between δW and R_{JB} values, expressed as

$$\delta W = \Delta c_3 \cdot (R_{\mathrm{JB}} - R_{\mathrm{ref}}) + \delta W_{lR}, \quad (3)$$

in which Δc_3 is the adjustment coefficient of anelastic attenuation, δW_{lR} is approximately the mean δW value at close distance, and the reference distance R_{ref} is fixed to be 1.0 km. To ensure a reliable regression, we limited the data range used in the regression to $R_{\mathrm{JB}} > 35$ km because data within $R_{\mathrm{JB}} = 35$ km are very few. The regressed lines for PGA and PSAs at periods of 0.2, 2.0, and 5.0 s were plotted in Figure 9a, and the Δc_3 values for PSA at different period ranging from 0.04 s to 5.0 s were provided in Figure 9b. It shows that the Δc_3 values are almost positive at entire period range, indicating the low-anelastic attenuation in the Jiuzhaigou and Lushan regions compared with the one both GMPEs account for.

Irrespective of GMPE selected, the regressed lines for PGA and PSAs at periods of 0.2 and 2.0 s are much steeper for the Jiuzhaigou event than for the Lushan earthquake, and the values of Δc_3 in the Jiuzhaigou event are considerably larger at short to intermediate periods (approximately < 3.0 s) than in the Lushan event but slightly smaller at long periods (approximately > 3.0 s). This exhibits the significantly slower anelastic attenuation effects on short- and intermediate-period ground motions in the Jiuzhaigou region than in the Lushan region, while the slightly stronger anelastic attenuation effects on long-period ground motions.

SIGNIFICANT DURATION

The significant duration, which is defined as the total time between the points at which 5% and 95% of the total Arias intensity are reached (Trifunac and Brady, 1975), denoted by D_{SR}(5%–95%), was calculated for all recordings in both earthquakes, as shown in Figure 10. The values of horizontal D_{SR}(5%–95%), that is, the geometrical mean of the two orthogonal horizontal components (east–west and north–south) in the Jiuzhaigou earthquake are listed in Ⓔ Table S1. The observed D_{SR}(5%–95%) values in both events were compared with the predicted medians provided by the GMPE developed by Afshari and Stewart (2016). The prediction was separately calculated at each station site using individual R_{rup} and V_{S30} values. Figure 10 shows that both earthquakes produced comparable durations of ground motions even though they produced con-

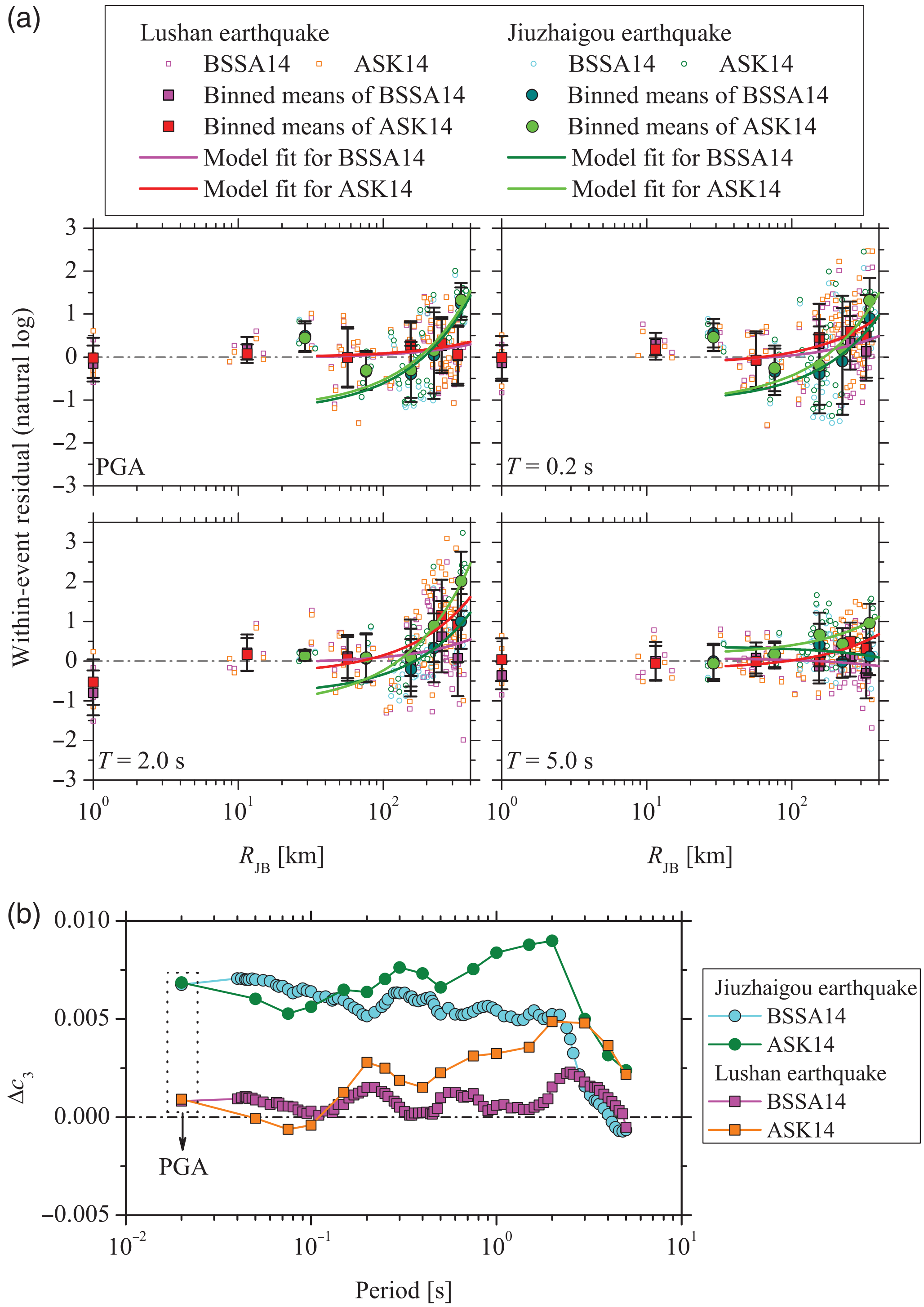

▲ **Figure 9.** (a) Within-event residuals for PGA and PSAs at periods of 0.2, 2.0, and 5.0 s plotted against R_{JB} for the Jiuzhaigou and Lushan earthquakes based on the BSSA14 and ASK14 GMPE models, respectively. Distance-binned medians with one standard deviation (error bars) are plotted for each earthquake. The trend lines of δW against R_{JB} were regressed linearly for each earthquake based on data in the $R_{JB} = 35$–400 km range. Circles on the vertical axis represent the four recordings obtained at stations with $R_{JB} = 0$ km in the Lushan earthquake. (b) Values of Δc_3 derived from the linear regression between δW and R_{JB} according to equation (3) for PGA and PSAs at periods ranging from 0.04 to 5.0 s.

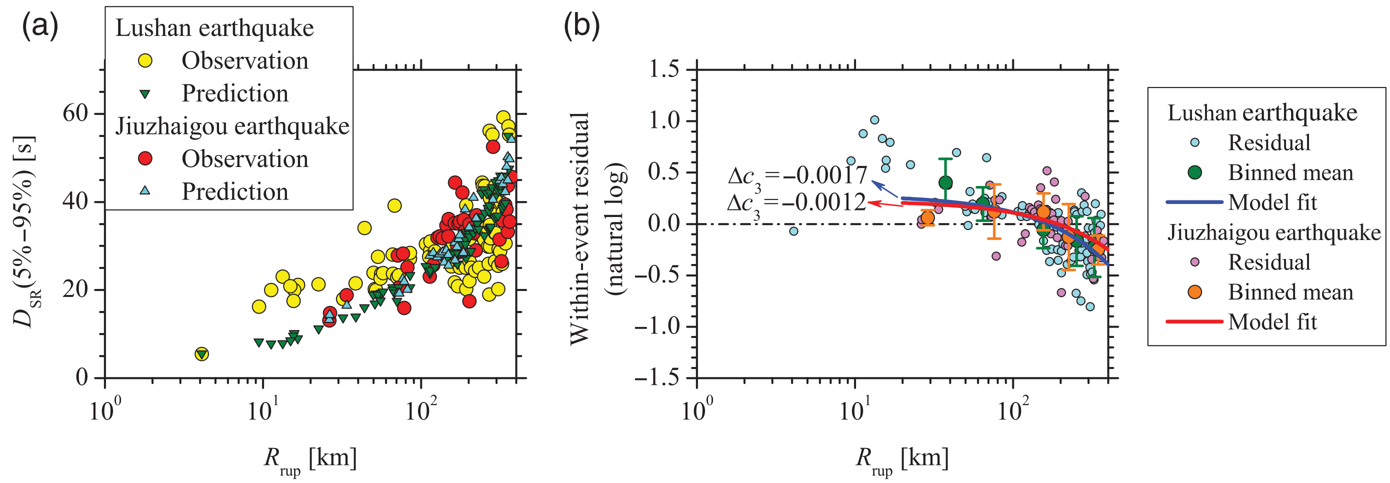

▲ **Figure 10.** (a) Comparison of the observed significant durations with the predicted medians by the GMPE of Afshari and Stewart (2016) for the Lushan and Jiuzhaigou earthquakes, respectively. (b) Within-event residuals for both earthquakes against R_{rup}. Distance-binned means with one standard deviation (error bars) are plotted for each earthquake. The trend lines of δW against R_{rup} were regressed linearly, and the resulting Δc_3 values are also shown.

siderably inconsistent PGAs, PGVs, and PSAs, as shown in Figures 6 and 7. The D_{SR}(5%–95%) in the Jiuzhaigou event was generally well predicted at sites for $R_{rup} < 300$ km but was mostly overestimated for $R_{rup} > 300$ km. For the Lushan event, the predicted medians are generally overestimated at many sites for $R_{rup} > \sim 150$ km but overall underestimated at sites for $R_{rup} < \sim 150$ km.

The values of δW were calculated and plotted in Figure 10b to investigate the potential dependence of D_{SR} on the distance in both events. As the same with the PGA and PSA, we fitted a linear expression between δW and R_{rup} values using the same form as equation (3), resulting in the approximate values of Δc_3 for Lushan and Jiuzhaigou events, that is, −0.0017 and −0.0012, respectively. The similar trends of within-event residuals against R_{rup} in both events indicate the similar dependence of D_{SR} on the distance in both the Lushan and the Jiuzhaigou regions.

CONCLUSIONS

In this study, we presented an introduction to the strong-motion observations of the M_s 7.0 Jiuzhaigou earthquake, which occurred on 8 August 2017, and investigated the characteristics of some ground-motion IMs, including PGA, PGV, PSAs, and D_{SR}(5%–95%). We compared these IMs with empirical predictions provided by GMPEs and with those observed in the M_s 7.0 Lushan earthquake on 20 April 2013 that also occurred in southwestern China to explore the differences of source, propagation path, and site effects on ground motions between both events.

In terms of the site conditions of the considered strong-motion stations in both events, similar V_{S30} distributions were observed, predominantly ranging from 350 to 400 m/s (classified as class II sites), implying approximately consistent site effects.

We observed that the PGAs, PGVs, and PSAs at short to intermediate periods in the Jiuzhaigou event were smaller than in the Lushan event for $R_{JB} < 200$ km. However, they appeared to present similar distributions at far-field sites ($R_{JB} > 200$ km). Intriguingly, larger PSAs at long periods were observed in the Jiuzhaigou event, irrespective of R_{JB}. According to analysis of the between-event residuals, we found that the source effect caused the larger long-period ground motions but smaller short- and intermediate-period ground motions in the Jiuzhaigou earthquake compared with the Lushan earthquake. Such period-dependent differences of ground motions between the two events may be attributable to their different centroid depths and fault types.

According to analysis of the within-event residuals, slower anelastic attenuation (i.e., high Q) for ground motions at short-to-intermediate periods was exhibited in the Jiuzhaigou region compared with the Lushan region, but both regions exhibited similar anelastic attenuation for ground motions at long periods. This shows that the observed ground-motion durations were comparable in both earthquakes and exhibited similar distance dependence in both regions.

DATA AND RESOURCES

The fatality and injury values were derived from http://www.cea.gov.cn/publish/dizhenj/468/553/101710/101716/20170814093548419970109/index.html (last accessed February 2018, in Chinese). The macroseismic intensity map was available at http://www.cea.gov.cn/publish/dizhenj/468/553/101710/101715/20170812212224652123547/index.html (last accessed February 2018, in Chinese). Strong-motion recordings used in this study were obtained from the China Strong-Motion Networks Center at http://www.csmnc.net (last accessed August 2017). The hypocentral location and the surface magnitude were derived from the China Earthquake Network Center (CENC; http://

news.ceic.ac.cn, last accessed October 2017). The Global Centroid Moment Tensot (CMT) project is available at http://www.globalcmt.org (last accessed August 2017). The V_{S30} values for some stations in west China were obtained from the Next Generation Attenuation (NGA) site database of the Pacific Earthquake Engineering Research Center and were available at http://peer.berkeley.edu/nga (last accessed August 2017). Some of the plots were produced using Generic Mapping Tools (Wessel and Smith, 1991).

ACKNOWLEDGMENTS

This work was partially supported by National Key R&D Program of China (Number 2017YFC1500802), Science Fund of Heilongjiang Province Number LC2015022, and National Natural Science Fund Numbers 51778589 and U1534202. We are very grateful to the two anonymous reviewers for their valuable suggestions and comments.

REFERENCES

Abrahamson, N. A., W. J. Silva, and R. Kamai (2014). Summary of the ASK14 ground motion relation for active crustal region, *Earthq. Spectra* **30,** 1025–1055, doi: 10.1193/070913EQS198M.

Afshari, K., and J. P. Stewart (2016). Physically parameterized prediction equations for significant duration in active crustal regions, *Earthq. Spectra* **32,** 2057–2081, doi: 10.1193/063015EQS106M.

Al Atik, L., N. Abrahamson, J. J. Bommer, F. Scherbaum, F. Cotton, and N. Kuehn (2010). The variability of ground-motion prediction models and its components, *Seismol. Res. Lett.* **81,** 794–801, doi: 10.1785/gssrl.81.5.794.

Ancheta, T. D., R. B. Darragh, J. P. Stewart, E. Seyhan, W. J. Silva, B. S.-J. Chiou, K. E. Wooddell, R. W. Graves, A. R. Kottke, D. M. Boore, *et al.* (2013). PEER NGA-West2 database, *PEER Report No. 2013/03*, Pacific Earthquake Engineering Research Center, University of California, Berkeley, California.

Bindi, D., F. Pacor, L. Luzi, R. Puglia, M. Massa, G. Ameri, and R. Paolucci (2011). Ground motion prediction equations derived from the Italian strong motion database, *Bull. Earthq. Eng.* **9,** 1899–1920, doi: 10.1007/s10518-011-9313-z.

Bommer, J. J., J. Douglas, and F. O. Strasser (2003). Style-of-faulting in ground-motion prediction equations, *Bull. Earthq. Eng.* **1,** 171–203.

Boore, D. M. (2010). Orientation-independent, nongeometric-mean measures of seismic intensity from two horizontal components of motion, *Bull. Seismol. Soc. Am.* **100,** 1830–1835, doi: 10.1785/0120090400.

Boore, D. M., J. P. Stewart, E. Seyhan, and G. M. Atkinson (2014). NGA-west2 equations for predicting PGA, PGV, and 5% damped PSA for shallow crustal earthquakes, *Earthq. Spectra* **30,** 1057–1085, doi: 10.1193/070113EQS184M.

GB 50011 (2010). *Code for Seismic Design of Buildings*, China Architecture Industry Press, Beijing, China (in Chinese).

GB/T 17742 (2008). *The Chinese Seismic Intensity Scale*, Standard Press of China, Beijing, China (in Chinese).

Han, L. B., J. Cheng, Y. R An, L. H. Fang, C. S Jiang, B. Chen, Z. L Wu, J. Liu, X. W. Xu, R. F Liu, *et al.* (2018). Preliminary report on the 8 August 2017 M_s 7.0 Jiuzhaigou, Sichuan, China, Earthquake, *Seismol. Res. Lett.* **89,** no. 2A, 557–569, doi: 10.1785/0220170158.

Han, L. B., X. F. Zeng, C. S. Jiang, S. D. Ni, H. J. Zhang, and F. Long (2014). Focal mechanisms of the 2013 M_w 6.6 Lushan, China earthquake and high-resolution aftershock relocations, *Seismol. Res. Lett.* **85,** 8–14, doi: 10.1785/0220130083.

Ji, K., Y. F. Ren, and R. Z. Wen (2017). Site classification for National Strong Motion Observation Network System (NSMONS) stations in China using an empirical H/V spectral ratio method, *J. Asian Earth Sci.* **147,** 79–94, doi: 10.1016/j.jseaes.2017.07.032.

Li, X. J., Z. H. Zhou, M. Huang, R. Z. Wen, H. Y. Yu, D. W. Lu, Y. N. Zhou, and J. W. Cui (2008). Preliminary analysis of strong-motion recordings from the magnitude 8.0 Wenchuan China, earthquake of 12 May 2008, *Seismol. Res. Lett.* **79,** 844–854, doi: 10.1785/gssrl.79.6.844.

Li, Z. W., S. D. Ni, T. Y. Hao, Y. Hu, and S. Roecker (2012). Uppermost mantle structure of the eastern margin of the Tibetan plateau from interstation *Pn* traveltime difference tomography, *Earth Planet. Sci. Lett.* **335/336,** 195–205, doi: 10.1016/j.epsl.2012.05.005.

Lyu, H. S., and F. X. Zhao (2007). Site coefficients suitable to China site category, *Acta Seismol. Sin.* **20,** 71–79.

Seyhan, E., J. P. Stewart, T. D. Ancheta, R. B. Darragh, and R. B. Graves (2014). NGA-West2 site database, *Earthq. Spectra* **30,** 1007–1024, doi: 10.1193/062913EQS180M.

Trifunac, M. D., and A. G. Brady (1975). A study on the duration of strong ground motion, *Bull. Seismol. Soc. Am.* **65,** 581–626.

Wang, C. Y., W. B. Han, J. P. Wu, H. Luo, and W. W. Chan (2007). Crustal structure beneath the eastern margin of the Tibetan plateau and its tectonics implications, *J. Geophys. Res.* **112,** no. B07307, doi: 10.1029/2005JB003873.

Wang, H. W., Y. F. Ren, and R. Z. Wen (2017). Source spectra of the 8 August 2017 Jiuzhaigou M_s 7.0 earthquake and the quality factor of the epicenter area, *Chin. J. Geophys.* **60,** 4117–4123, doi: 10.6038/cjg20171036 (in Chinese).

Wang, W. M., J. L. Hao, and Z. X. Yao (2013). Preliminary result for rupture process of Apr. 20, 2013, Lushan earthquake, Sichuan, China, *Chin. J. Geophys.* **56,** 1412–1417 (in Chinese).

Wen, R. Z., and Y. F. Ren (2014). Strong-motion observations of the Lushan earthquake on 20 April 2013, *Seismol. Res. Lett.* **85,** 1043–1055, doi: 10.1785/0220140006.

Wessel, P., and W. H. F. Smith (1991). Free software helps map and display data, *Eos Trans. AGU* **72,** 441.

Xu, X. W., G. H. Chen, Q. X. Wang, L. C. Chen, Z. K. Ren, C. Xu, Z. Y. Wei, R. Q. Lu, X. B. Tan, S. P. Dong, *et al.* (2017). Discussion on seismogenic structure of Jiuzhaigou earthquake and its implication for current strain state in the southeastern Qinghai-Tibet plateau, *Chin. J. Geophys.* **60,** 4018–4026, doi: 10.6038/cjg20171028 (in Chinese).

Yi, G. X., F. Long, M. J. Liang, H. P. Zhang, M. Zhao, Y. Q. Ye, Z. W. Zhang, Y. P. Qi, S. W. Wang, Y. Gong, *et al.* (2017). Focal mechanism, solutions and seismogenic structure of the 8 August 2017 M 7.0 Jiuzhaigou earthquake and its aftershocks, northern Sichuan, *Chin. J. Geophys.* **60,** 4083–4097, doi: 10.6038/cjg20171033 (in Chinese).

Zhang, Y., L. S. Xu, and Y. T. Chen (2017). Earthquake of magnitude 7.0 in Jiuzhaigou, Sichuan on August 8, 2017, available at http://www.cea-igp.ac.cn/tpxw/275883.html (last accessed October 2017).

Yefei Ren
Hongwei Wang
Peibin Xu
Ruizhi Wen
Qiang Ma
Key Laboratory of Earthquake Engineering and Engineering Vibration of China Earthquake Administration
Institute of Engineering Mechanics, China Earthquake Administration
No. 29 Xuefu Road
Harbin 150080, China

renyefei@iem.ac.cn
whw1990413@163.com
xupeibin13@126.com
ruizhi@iem.ac.cn
maqiang@iem.ac.cn

Yadab P. Dhakal
National Research Institute for Earth Science and Disaster Resilience
3-1, Tennodai, Tsukuba
Ibaraki 305-0006, Japan
ydhakal@bosai.go.jp

Peng Jiang
Sichuan Earthquake Administration
No 29, South Renmin Road
Chengdu 610000, China
jiang_0057@163.com

Published Online 30 May 2018